Multidimensional Signal Processing Methods: Target Detection Methods Based on Tensor Decompositions

CAROLINE FOSSATI
caroline.fossati@fresnel.fr
SALAH BOURENNANE
salah.bourennane@fresnel.fr
Aix Marseille Univ, CNRS, Centrale Marseille, Institut Fresnel, Marseille, France

Abstract: Reducing noise is an important preprocessing step for further analyze the information in the hyperspectral image (HSI). Commonly, filtering methods for HSIs are based on the data vectorization or matricization while ignore the related information between different bands. So there are new approaches considering multidimensional data as whole entities based on tensor decomposition. However, it can not cope with the HSIs disturbed by non-white noise which is the most cases in the actual world and cannot preserve small targets. In this paper, we propose a new method for the reduction of non-white noise from images. The first step of this method is to change the noise in HSIs being a white one through a prewhitening procedure(PW). Then multidimensional wavelet packet transform with multiway Wiener filter (PW-MWPT-MWF) to improve the target detection efficiency of HSI with small targets in the noise environment. The performances of the our method (PW-MWPT-MWF) are exemplified using simulated and real-world HSI

Key–Words: Prewhitening, Hyperspectral image; small target detection; multiway Wiener Filter

1 Introduction

A hyperspectral image is a multidimensional array also named as a tensor and it normally consists of hundreds of spectral bands. So, HSI data, for instance, airborne hyperspectral images HYDICE (Hyperspectral Digital Imagery Collection Experiment) [4], has two spatial dimensions and one spectral dimen- sion. While acquired images in hyperspectral imagery are disturbed by additive noise, which can degrade classifcation and target detection results. To reduce the noise, HSI is commonly split into vectors or matrix so any 2D filtering method could be applied, but this splitting way dose not consider the related information between image planes [14]. So, some new approaches, such as tensor decomposition method, has been used to denoise those images and showed some prospects in this field. There are two main decomposition models for multidimensional arrays: TUCKER3 (Three-mode factor analysis) decomposition and PARAFAC/CANDECOMP (Canonical Decomposition / Parallel Factor Analysis) decomposition [7, 8].

A multiway Wiener filter (MWF) [3, 11–13] is proposed to process a HSI as a whole entity based on TUCKER3 decomposition [7, 8]. In MWF, the filter in each mode is computed as a function of the filters in other modes, which reflects its capability in integrally utilizing the information in each mode of the multidimensional data. In practice, HSIs are always disturbed by hard-removed non-white noise, but this MWF method could not deal with the cases with non-white noise. So a prewhitening procedure for HSIs to change the non-white noise to a white one is proposed in this paper. After that MWF can be used to filter the prewhitened result (PW-MWF). Then we can get the denoised images by an inverse processing of prewhitening. Though PW-MWF preserves the data structure of HSI, it also has some negative side effects in preserving small targets in the denoising process. In fact, PW-MWF is essentially an optimal low-pass filter while small targets are high frequency signals in Fourier basis, therefore PW-MWF might remove small targets in the denoising process. A multidimensional wavelet packet transform decomposes the prewhitened HSI into different coefficient tensors (components) by wavelet packet transform [6], and jointly filter each component by MWF.

Since small target detection is an important issue in the HSI processing field [1, 10], in this paper, PW-MWPT-MWF is proposed to reduce non-white noise in HSI with small targets and hence improve the target detection performances. The experiments of simulated and real-world images are given to present the performances of target detection after denoising by PW-MWPT-MWF.

The remainder of the paper is as follows: Section 2 introduces some basic knowledge about the multilinear algebra. Section 3 introduces the signal model. Section 4 introduces the proposed prewhitening algorithm. Section 5 shows how to use MWF to jointly

filter the data component tensor. Section 6 presents some experimental results and finally section 7 concludes this paper.

2 Multilinear algebra tools

2.1 n-mode unfolding

The n-mode vectors are the I_n-dimensional vectors obtained from a tensor by varying index i_n while keeping the other indices fixed. The so-called n-mode flattened matrix $\mathbf{X}_n \in \mathbb{R}^{I_n \times M_n}$ $(n = 1, 2, 3)$ denotes the n-mode unfolding matrix of a tensor $\mathbf{X} \in \mathbb{R}^{I_1 \times I_2 \times I_3}$, with size $I_n \times M_n$ where $M_n = I_p \times I_q$ with $p, q \neq n$ $(p, q = 1, 2, 3)$. The columns of $\mathbf{X}_n$ are the I_n-dimensional vectors obtained from $\mathbf{X}$ by varying index i_n while keeping the other indices fixed.

2.2 n-mode product

The n-mode product of a data tensor $\mathbf{X} \in \mathbb{R}^{I_1 \times \ldots \times I_N}$ and a matrix $\mathbf{B} \in \mathbb{R}^{J \times I_n}$ in mode n. It is of size $I_1 \times \cdots \times I_{n-1} \times J \times I_{n+1} \times \cdots \times I_N$ and denoted by $\mathbf{X} \times_n \mathbf{B}$,is a tensor in which the entries are given by $(\mathbf{X} \times_n \mathbf{B})_{i_1, \cdots i_{n-1}, j, i_{n+1}, \cdots i_N} = \sum_{i_n=1}^{I_n} x_{i_1, i_2, \cdots i_N} b_{j, i_n}$ where b_{j,i_n} denotes the (j, i_n) element of matrix $\mathbf{B}$ and $j = 1, \cdots J$.

2.3 Signal model

A noisy HSI is modeled as a tensor $\mathbf{R} \in \mathbb{R}^{I_1 \times I_2 \times I_3}$ resulting from a pure HSI $\mathbf{X} \in \mathbb{R}^{I_1 \times I_2 \times I_3}$ impaired by an additive tensor noise $\mathbf{N} \in \mathbb{R}^{I_1 \times I_2 \times I_3}$. The tensor $\mathbf{R}$ can be expressed as

$$\mathbf{R} = \mathbf{X} + \mathbf{N} \tag{1}$$

3 Noise reduction by joint component filtering

3.1 Three-dimensional wavelet packet transform

The 3-dimensional wavelet packet transform (3D-WPT) can be computed by performing 1-D wavelet packet transform in each mode. Therefore, the wavelet packet coefficient tensor $\mathbf{C}^{\mathbf{R}}$ can be computed as: $\mathbf{C}^{\mathrm{R}} = \mathbf{R} \times_1 \mathbf{W}_1 \times_2 \mathbf{W}_2 \times_3 \mathbf{W}_3 = (\mathbf{X} + \mathbf{N}) \times_1 \mathbf{W}_1 \times_2 \mathbf{W}_2 \times_3 \mathbf{W}_3$ Therefore, the coefficient tensor of each part: $\mathbf{C}^{\mathrm{X}} = \mathbf{X} \times_1 \mathbf{W}_1 \times_2 \mathbf{W}_2 \times_3 \mathbf{W}_3$ and $\mathbf{C}^{\mathrm{N}} = \mathbf{N} \times_1 \mathbf{W}_1 \times_2 \mathbf{W}_2 \times_3 \mathbf{W}_3$ and the reconstruction can be written as:

$$\mathbf{R} = \mathbf{C}^{\mathrm{R}} \times_1 \mathbf{W}_1{}^{\mathrm{T}} \times_2 \mathbf{W}_2^{\mathrm{T}} \times_3 \mathbf{W}_3^{\mathrm{T}} \tag{2}$$

where $\mathbf{W}_n \in \mathbb{R}^{I_n \times I_n}, n = 1, 2, 3$ indicate the wavelet packet transform matrices and the superscript T denotes the transpose. When the transform level vector is $\mathbf{l} = [l_1, l_2, l_3]^T$, where $l_n \geq 0$ denotes the wavelet packet transform level in mode n, the coefficient tensor $\mathbf{C}^{\mathbf{R}}_{\mathbf{l},\mathbf{m}}$, which is also called a component in this paper, of scale $\mathbf{m} = [\mathbf{m_1}, \mathbf{m_2}, \mathbf{m_3}]$, where $0 \leq m_n \leq 2^{l_n} - 1$, can be extracted by: $\mathbf{C}^{\mathrm{R}}_{\mathbf{l},\mathbf{m}} = \mathbf{C}^{\mathrm{R}} \times_1 \mathbf{E}_{m_1} \times_2 \mathbf{E}_{m_2} \times_3 \mathbf{E}_{m_3} = (\mathbf{C}^{\mathbf{X}} + \mathbf{C}^{\mathbf{N}}) \times_1 \mathbf{W}_1{}^T \times_2 \mathbf{W}_2^T \times_3 \mathbf{W}_3^T$. Then, $\mathbf{C}^{\mathbf{R}}_{\mathbf{l},\mathbf{m}}$ can be expressed as $\mathbf{C}^{\mathbf{R}}_{\mathbf{l},\mathbf{m}} = \mathbf{C}^{\mathbf{X}}_{\mathbf{l},\mathbf{m}} + \mathbf{C}^{\mathbf{N}}_{\mathbf{l},\mathbf{m}}$ where $\mathbf{C}^{\mathbf{X}}_{\mathbf{l},\mathbf{m}} = \mathbf{C}^{\mathbf{X}} \times_1 \mathbf{W}_1{}^T \times_2 \mathbf{W}_2^T \times_3 \mathbf{W}_3^T$ and $\mathbf{C}^{\mathbf{N}}_{\mathbf{l},\mathbf{m}} = \mathbf{C}^{\mathbf{N}} \times_1 \mathbf{W}_1{}^T \times_2 \mathbf{W}_2^T \times_3 \mathbf{W}_3^T$ are the signal and noise coefficient tensors, respectively. The corresponding inverse process is

$$\mathbf{C}^{\mathbf{R}} = \sum_{m_1} \sum_{m_2} \sum_{m_3} \mathbf{C}^{\mathbf{R}}_{\mathbf{l},\mathbf{m}} \times_1 \mathbf{E}_{m_1}^T \times_2 \mathbf{E}_{m_2}^T \times_3 \mathbf{E}_{m_3}^T \tag{3}$$

where the extraction operator $\mathbf{E}_{m_n}$ is defined as: $\mathbf{E}_{m_n} = [\mathbf{0}_1, \mathbf{I}_{\frac{I_n}{2^{l_n}} \times \frac{I_n}{2^{l_n}}}, \mathbf{0}_2] \in \mathbb{R}^{I_n/2^{l_n} \times I_n}$ where $\mathbf{0}_1$ is a zero matrix with size $\frac{I_n}{2^{l_n}} \times \frac{m_n I_n}{2^{l_n}}$, $\mathbf{0}_2$ is a zero matrix with size $\frac{I_n}{2^{l_n}} \times \frac{(2^{l_n} - 1 - m_n) I_n}{2^{l_n}}$ and $\mathbf{I}_t$ is an identity matrix of size t .

4 Pre-whitening method

If the noise in HSI is not white, MWF cannot effectively remove the non-white noise and estimate the expected signal. In this paper, we propose to change the non-white noise in $\mathcal{R}$ into a white one by a preprocessing procedure, then MWF can be used to denoise the whitened data tensor $\overline{\mathcal{R}}$.

If the noise in HSI is not white, the noise covariance matrix $\mathbf{C}_{\mathcal{N}}^{(n)} \neq \sigma^2 \mathbf{I}$, where σ^2 is the variance of the corresponding white noise, then a prewhitening matrix $\mathbf{P}_n^{-1}$ can be applied to $\mathcal{R}$. The matrix $\mathbf{P}_n$ is given by $\mathbf{C}_{\mathcal{N}}^{(n)} = \mathbf{P}_n^T \mathbf{P}_n$, where $\mathbf{P}_n$ is the Cholesky factor of $\mathbf{C}_{\mathcal{N}}^{(n)}$. If we can directly get the unfolding matrix $\mathbf{N}_n$ of the noise tensor $\mathcal{N}$, then it can be factored as $\mathbf{N}_n = \mathbf{Q}_n \mathbf{P}_n$, where $\mathbf{Q}_n^T \mathbf{Q}_n = \mathbf{I}$ and $\mathbf{P}_n$ is the same Cholesky factor as above. In the non-white noise case, we consider the unfolding matrix $\mathbf{R}_n = \mathbf{X}_n + \mathbf{N}_n$ and substitute $\mathbf{R}_n$ to $\overline{\mathbf{R}}_n = \mathbf{R}_n \mathbf{P}_n^{-1}$, then

$$\overline{\mathbf{R}}_n = \mathbf{X}_n \mathbf{P}_n^{-1} + \mathbf{N}_n \mathbf{P}_n^{-1} = \mathbf{X}_n \mathbf{P}_n^{-1} + \mathbf{Q}_n \tag{4}$$

with the assumption that the signal is independent of the noise.

So, the covariance matrix $\overline{\mathbf{R}}_n^T \overline{\mathbf{R}}_n = (\mathbf{P}_n^{-1})^T \mathbf{X}_n^T \mathbf{X}_n \mathbf{P}_n^{-1} + \mathbf{I}$, that is to say that the non-white noise has been whitened. Thus the MWF

algorithm can be applied to the transformed unfolding data matrix $\mathbf{R}_n\mathbf{P}_n^{-1}$. This procedure is named as PW-MWF. To get the estimated signal $\hat{\mathcal{X}}$, an inverse process of prewhitening is necessary after we get the denoised result, which will be described in the next subsections.

Notice that the large and small targets are separated into the approximation and detail coefficient tensors respectively, which makes it possible to avoid removing the small target in filtering noise. Therefore, PW-MWPT-MWF outperforms PW-MWF in preserving the small targets.

5 Experimental results

In the experiments, PW-MWPT-MWF and PW-MWF are compared in the aspect of improving target detection performances. The results obtained both on simulated and real-world data are presented in this section. The HSI is modeled as a three-dimensional tensor, where the first two dimensions indicate the spatial field and the third dimension indicates the spectral bands. Wavelet db3 is used to apply PW-MWPT-MWF with transform levels $[l_1, l_2, l_3] = [1, 1, 0]$.

SAM detector [9] is used in the experiments to detect targets in the image. As Spectral Angle Mapper (SAM) does not require the characterization of background, it can avoid the inaccuracy of the comparison result caused by the noise covariance matrix estimation error. The SAM detector can be expressed as:

$$T_{SAM}(\mathbf{x}) = \frac{\mathbf{s^T x}}{(\mathbf{s^T s})^{1/2}(\mathbf{x^T x})^{1/2}} \tag{5}$$

where $\mathbf{s}$ is the reference spectrum, $\mathbf{x}$ is the pixel spectrum. To assess the performances of detection, the probability of detection (Pd) is defined as:

$$Pd = \frac{\sum_i^{n_s} N_i^{rd}}{\sum_i^{n_s} N_i} \tag{6}$$

and the probability of false alarm (Pfa) is defined as:

$$Pfa = \frac{\sum_i^{n_s} N_i^{fd}}{\sum_i^{n_s} (I_1 \times I_2 - N_i)} \tag{7}$$

where n_s is the number of spectral signatures, N_i the number of pixels with spectral signature i, N_i^{rd} the number of rightly detected pixels, and N_i^{fd} the number of falsely detected pixels.

5.1 Results on simulated data

The simulated data is generated with the spectral signatures presented in Fig. 1 and it has 100 rows, 100 columns and 220 spectral bands, which can be modeled as a $100 \times 100 \times 220$ tensor. There are six target types and three different spatial sizes 8×8, 3×3, 1×1 of each type, which are shown in Fig. 2(a). These targets are mixed to the background by using the linear mixing model with target abundance being 80%. The band 6 of the noisy image with SNR= 20dB is shown Fig. 2(b), from which one can see that the small targets are almost disappeared in the noise.

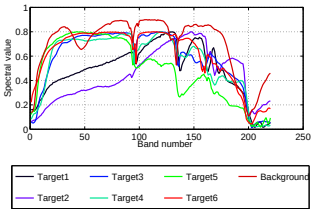

Figure 1: Spectral signatures of the simulated data

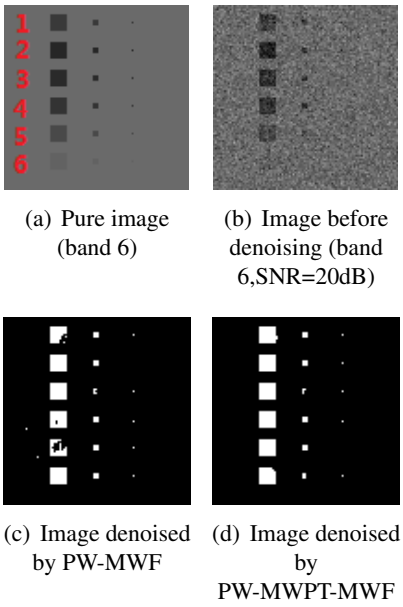

(a) Pure image (band 6)
(b) Image before denoising (band 6,SNR=20dB)
(c) Image denoised by PW-MWF
(d) Image denoised by PW-MWPT-MWF

Figure 2: Detection results of HYDICE, Pfa=10^{-4}

Fig. 2(c) shows the detection result under Pfa $= 10^{-4}$ after denoising by PW-MWF. In this figure, it is obvious that most of the 1×1 targets are not detected and there are false alarm neighbors with the detected 1×1 targets. On the contrast, the detection result after denoising by PW-MWPT-MWF is much better. The 2×2 targets are all detected and only one 1×1 target is dismissed. The experiment result in Fig. 2 implies that PW-MWPT-MWF owns the capability in preserving the small targets in the denoising process.

To make the experimental results more convincing and show the subtle changes of the detection results, the receiver operating characteristic (ROC) values are given in Table 1 in the noise environments

Table 1: ROC values of PW-MWF and PW-MWPT-MWF for the simulated HSI

Pfa	Pd of PW-MWF			Pd of PW-MWPT-MWF		
	15dB	20dB	25dB	15dB	20dB	25dB
0.0001	0.515	0.9492	0.9863	0.7125	0.9282	0.9675
0.0002	0.581	0.9492	0.9863	0.7271	0.9282	0.9678
0.0003	0.599	0.9493	0.9863	0.7381	0.9282	0.9775
0.0005	0.629	0.9494	0.9872	0.7637	0.9482	0.9779
0.0008	0.673	0.9494	0.9872	0.7821	0.9482	0.9872
0.0013	0.718	0.9515	0.9872	0.8004	0.9482	0.9876
0.0022	0.737	0.9515	0.9872	0.8132	0.9582	0.9973
0.0036	0.710	0.9515	0.9872	0.8462	0.9582	0.9989
0.0060	0.815	0.9589	0.9872	0.8956	1.0000	1.0000
0.0100	0.911	0.9845	1.0000	0.9908	1.0000	1.0000

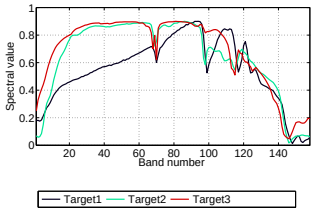

Figure 3: Spectral signatures of targets

from 15dB to 25dB. In 15dB, Pd after denoising by PW-MWPT-MWF is much greater than that by PW-MWF under the same Pfa. From the comparison of ROC in Table 1, it shows that PW-MWPT-MWF can improve the target detection performances more greatly than PW-MWF can in different noise environments.

5.2 Results on real-world data

One high spatial resolution HSI HYDICE [2] is denoised by PW-MWF and PW-MWPT-MWF to compare their target detection improvement ability in noise environment. The HYDICE image contains 100 rows, 100 columns and 158 spectral bands, which is modeled as a $100 \times 100 \times 158$ tensor. Three types of target spectral signatures are considered, and these targets are mixed to the background with respect to the linear mixing model when target abundance is 80%;

Table 2: ROC values of PW-MWF and PW-MWPT-MWF for HYDICE

Pfa	Pd of PW-MWF			Pd of PW-MWPT-MWF		
	15dB	20dB	25dB	15dB	20dB	25dB
0.0001	0.6593	0.8828	0.9634	0.7289	0.8851	0.9854
0.0002	0.6593	0.9048	0.969	0.7399	0.9084	0.9863
0.0003	0.6630	0.9121	0.9681	0.7546	0.9451	0.9866
0.0005	0.6703	0.9121	0.9734	0.7912	0.9634	0.9873
0.0008	0.6740	0.9487	0.985	0.7985	0.9670	0.9878
0.0013	0.6777	0.9634	0.989	0.8315	0.9707	0.989
0.0022	0.6850	0.9780	0.999	0.8498	0.9853	0.9899
0.0036	0.6923	1.0000	1.0000	0.8755	0.9927	0.9953
0.0060	0.7106	1.0000	1.0000	0.9341	0.9927	1.0000
0.0100	1.0000	1.0000	1.0000	1.0000	1.0000	1.0000

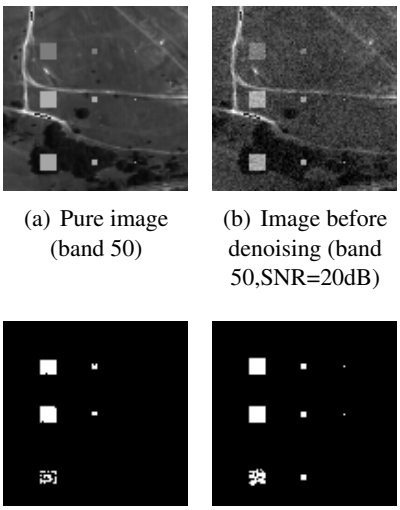

(a) Pure image (band 50)
(b) Image before denoising (band 50,SNR=20dB)
(c) Image denoised by PW-MWF
(d) Image denoised by PW-MWPT-MWF

Figure 4: Detection results of HYDICE, Pfa=10^{-4}

Fig. 4(a) and Fig. 4(d) are the pure and noisy images in band 50. The targets are placed in the field, beside the road and in the trees respectively to contain the usual target situations in HSI. The detection results after denoising by PW-MWF and PW-MWPT-MWF are shown in Fig. 4(c) and Fig. 4(d) respectively. In Fig. 4(d), 1×1 targets in the field and beside the road are detected. The only dismissed 1×1 target is in the trees, which is always a difficult situation to detect small target in it. On the contrast, in Fig. 4(c) all the 1×1 targets are dismissed and a 2×2 target in the trees is also lost. The comparison between Fig. 4(c) and Fig. 4(d) shows that PW-MWPT-MWF owns better capability in preserving small targets than PW-MWF as expected.

Apart from the binary target detection results in Fig. 4, to better compare the performances of PW-MWF and PW-MWPT-MWF, the ROC values are also presented in Table 2. As expected, the Pd of PW-MWPT-MWF is better than that of PW-MWF in the same Pfa. The comparison of the ROC values implies that PW-MWPT-MWF performs better than PW-MWF in improving the target detection result of the real-world data as well.

6 Conclusion

To reduce non-white noise in HSI, a pre-whitening method is proposed by a two-stage process comprised of a noise pre-whitening procedure and a MWF process. The performances of PW-MWF and PW-

MWPT-MWF in improving the target detection in noisy environment are discussed in this paper. Though PW-MWF performs well in reducing white noise in HSI, it might also remove targets in the image, especially when the targets are small. The reason leading to this phenomenon is that PW-MWF treats directly HSI as a whole entity by filtering each mode of the HSI in a Wiener filter like way. Since the energy of the small targets is thin, it is easy to be removed in the filtering process. However, PW-MWPT-MWF decompose the pre-whitening HSI into several components (coefficient tensors) and filter each one by MWF. As small and large targets are separated into different components, the small ones can be preserved in the filtering process. This is why PW-MWPT-MWF performs better than PW-MWF in improving target detection performance when there exist small targets in the image.

Simulated and real-world HSIs are considered in the experiments to compare the performances of PW-MWF and PW-MWPT-MWF in improving target detection in the noise environment. The experimental results highlight that PW-MWPT-MWF outperforms PW-MWF in improving the target detection results in the presence of small targets.

References:

[1] Acito, N., Diani, M., Corsini, G.: A new algorithm for robust estimation of the signal subspace in hyperspectral images in the presence of rare signal components. IEEE Trans. Geosci. Remote Sens. 47(11), 3844–3856 (2009)

[2] Basedow, R.W., Carmer, D.C., Anderson, M.E.: Hydice system: Implementation and performance. In: SPIE's 1995 Symposium on OE/Aerospace Sensing and Dual Use Photonics. pp. 258–267. International Society for Optics and Photonics (1995)

[3] Bourennane, S., Fossati, C., Cailly, A.: Improvement of classification for hyperspectral images based on tensor modeling. IEEE Geosci. Remote Sens. Lett. 7(4), 801–805 (2010)

[4] Bourennane, S., Fossati, C., Cailly, A.: Improvement of target detection based on tensorial modelling. In: EUSIPCO. pp. 304–308 (Aug 2010)

[5] Cichocki, A., Zdunek, R., Phan, A., Amari, S.: Nonnegative matrix and tensor factorizations: applications to exploratory multi-way data analysis and blind source separation. Wiley, New Jersey (2009)

[6] Daubechies, I.: Ten lectures on wavelets. SIAM (2006)

[7] De Lathauwer, L., De Moor, B., Vandewalle, J.: A multilinear singular value decomposition. SIAM J. Matrix Anal. Appl. 21(4), 1253–1278 (2000)

[8] De Lathauwer, L., De Moor, B., Vandewalle, J.: On the best rank-1 and rank-(r1,r2,..., rn) approximation of higher-order tensors. SIAM J. Matrix Anal. Appl.21(4), 1324–1342 (2000)

[9] Jin, X., Paswaters, S., Cline, H.: A comparative study of target detection algorithms for hyperspectral imagery. In: SPIE Defense, Security, and Sensing. pp. 73341W–73341W. International Society for Optics and Photonics (2009)

[10] Kuybeda, O., Malah, D., Barzohar, M.: Rank estimation and redundancy reduction of high-dimensional noisy signals with preservation of rare vectors. IEEE Trans. Signal Process. 55(12), 5579–5592 (2007)

[11] Letexier, D., Bourennane, S.: Noise removal from hyperspectral images by multidimensional filtering. IEEE Trans. Geosci. Remote Sens. 46(7), 2061–2069 (2008)

[12] Letexier, D., Bourennane, S., Blanc-Talon, J.: Nonorthogonal tensor matricization for hyperspectral image filtering. IEEE Geosci. Remote Sens. Lett. 5(1), 3–7 (2008)

[13] Muti, D., Bourennane, S.: Multidimensional filtering based on a tensor approach. Signal Process. 85(12), 2338–2353 (2005)

[14] Renard, N., Bourennane, S.: Improvement of target detection methods by multiway filtering. IEEE Trans. Geosci. Remote Sens. 46(8), 2407–2417 (2008)